*Science of Sintering,* **50** (2018) 291-298

doi: https://doi.org/10.2298/SOS1803291S

UDK 546.824; 53.086

# The Effect of Sintering Temperatures of $TiO_2$(B)-Nanotubes on Its Microstructure

**H. Sutrisno[*)], E. D. Siswani, K. S. Budiasih**
Department of Chemistry Education, Faculty of Mathematics and Natural Sciences, Yogyakarta State University (YSU), Kampus Karangmalang, Jl. Colombo No.1, Yogyakarta 55281, Indonesia

***Abstract:***

*Titanium dioxide ($TiO_2$)-nanotubes were prepared by a simple technique reflux. The morphologies and microstructures of nanotubes were characterized by high resolution scanning electron microscopy (HRSEM), high resolution transmission electron microscopy (TEM), powder X-ray diffraction (XRD,) energy dispersive X-ray spectroscopy (EDS) and surface area analyzer. The microstructures of $TiO_2$ phases obtained from the sintering process of $TiO_2$-nanotubes for 1 hour at various temperatures from 100 to 1000 °C at intervals of 50 °C were investigated from the XRD diffractograms. The analyses of morphologies and microstructures from HRSEM and HRTEM images describe the sample as nanotubes. The nanotube is single phase exhibiting $TiO_2$(B) structure. The XRD patterns show that $TiO_2$(B)-nanotubes transform into anatase phase and then become rutile due to increasing sintering temperatures.*

***Keywords:*** *Titanium dioxide; Anatase; Rutile; Microstructure; Nanotubes.*

## 1. Introduction

Among all transition-metal oxides, titania or titanium dioxide ($TiO_2$) has a wide range of applications because of its excellent optical transmittance, high refractive index non-toxic, environmentally friendly, corrosion-resistant material and inert chemical properties. $TiO_2$ in all its crystal forms is a wide-bandgap semiconductor (Eg ≈3 eV) with suiTab. band-edge positions that enable its use in solar cells or photovoltaic devices [1-3], in photocatalytic reactions [4-5], and antibacterial purposes [6-7]. Photogenerated electron-hole pairs can be used for splitting water into oxygen and hydrogen, or can be used for the remediation of hazardous wastes, such as contaminated ground waters, or the control of toxic air contaminants, for super hydrophilic and light-induced amphiphilic surfaces [8-13].

The two most commonly synthesized $TiO_2$ structures are the low-temperature, anatase (***I4₁/amd***, tetragonal) [14] and the high-temperature, thermodynamically sTab. rutile form (***P4₂/mnm***, tetragonal) [15], though a second metasTab. $TiO_2$ variant brookite (***P****bca*, orthorhombic) [16] and $TiO_2$(B) (**C***2/m*, monoclinic) [17] are sometimes observed. The kinetically sTab. anatase phase is nearly four times more photocatalytically active than rutile $TiO_2$ phase, though mixed phase materials can be more active than pure anatase, and rutile nanoparticles show oxidative catalytic activity.

[*)] **Corresponding author**: sutrisnohari@uny.ac.id

Recently, $TiO_2$ materials with low dimensional (1D), such as nanoribbons, nanofibers, nanowires and nanotubes have attracted the interest of researchers and users because of its unique microstructure, surface area, morphology and function. Low-dimensional (1D) $TiO_2$-related materials prepared by chemical process are particularly interesting, because of their large specific surface area. Therefore, this material was developed as a photocatalyst, environmental purification, solar cells, gas and humidity sensors [18-21]. $TiO_2$-nanotube was first successfully synthesized by Kasuga et al. by treating $TiO_2$ in 10 M NaOH solution for 20 h at 110 °C [22]. In this paper, a simple technique reflux was applied to synthesize $TiO_2$(B)-nanotube materials. The effect of in-situ sintering temperatures of $TiO_2$(B)-nanotubes on its microstructure were investigated.

## 2. Experimental

### 2.1. Synthesis of $TiO_2$(B)-nanotubes

In these experiments, all the reagents were used without purification. Powder of $Ti(O_2)O.2H_2O$ was obtained from the reaction of $TiCl_4$ (Merck) and $H_2O_2$ (Merck) at atmosphere of $N_2$ gas [23]. A total of 5 g of $Ti(O_2)O.2H_2O$ and 100 mL of 10M NaOH solution were put into a polypropylene boiling flask. The suspension was stirred at room temperature for 2 h, then it was heated with a magnetic stirrer in reflux equipment at 150 °C for 24 h. The powder was filtered in the vacuum, washed by distilled water, and dried at 100 °C for 2 h.

### 2.2. Influence of Sintering Temperatures

The obtained powder was put into 100 mL of 0.1 M HCl solution and stirred for 5 h. The suspension was filtered and washed by distilled water until the washing water showed pH~6-7. After the washing treatment, it was filtered and subsequently dried at 70 °C for 20 h in an oven. The $TiO_2$ nanotube particles were sintered for 1 h from 100 to 1000 °C at interval of 50 $^oC$ and then the corresponding powder XRD at each temperature was recorded.

### 2.3. Characterization methods

The surface morphology of $TiO_2$-nanotubes were observed using a high resolution scanning electron microscope (HRSEM) JEOL 6400-F with a tungsten cathode field emission gun operating at 8 kV, while the morphologies and microstructures were investigated with a Hitachi HNAR-9000 high temperature resolution electron microscope (HRTEM) using 300 kV accelerating voltage.

Diffraction patterns of all products were collected using a Siemens D5000 diffractometer, operating in the Bragg configuration using Cu Kα radiation ($\lambda$ = 1.5406 Å) from 5 to 80° at scanning rates of 0.3° per min. The accelerating voltage and the applied current were 40 kV and 30 mA, respectively.

The porous structure characteristics were obtained from the conventional analysis of nitrogen adsorption-desorption isotherms measured at 77 K with Micromeritics ASAP 2020 instrument. The product was degassed at 100 °C prior to BET (Brunauer-Emmett-Teller) measurements [24]. The BET specific surface area ($S_{BET}$) was determined by a multipoint BET method using the adsorption data in the relative pressure ($P/P0$) of ~ 0.30. The desorption isotherm was used to determine the pore size distribution using the Barret-Joyner-Halender (BJH) method [25]. The nitrogen adsorption volume at the relative pressure ($P/P0$) of ~ 0.96 was used to determine the pore volume and the average pore size.

## 3. Result and discussion

### 3.1. Characterization of $TiO_2$(B)-nanotubes

The HRSEM images of the obtained product show large quantity of tubular materials with narrow size distribution (Fig. 1a). The image shows typical structure observed throughout the powder indicating that the yield of nanotubes from the technique reflux in the synthesis is high. The EDS analysis (Fig. 1b) reveals the presence of Ti and O elements in the nanotubes which were found in the mol ratio of Ti/O to be 0.901/2.008.

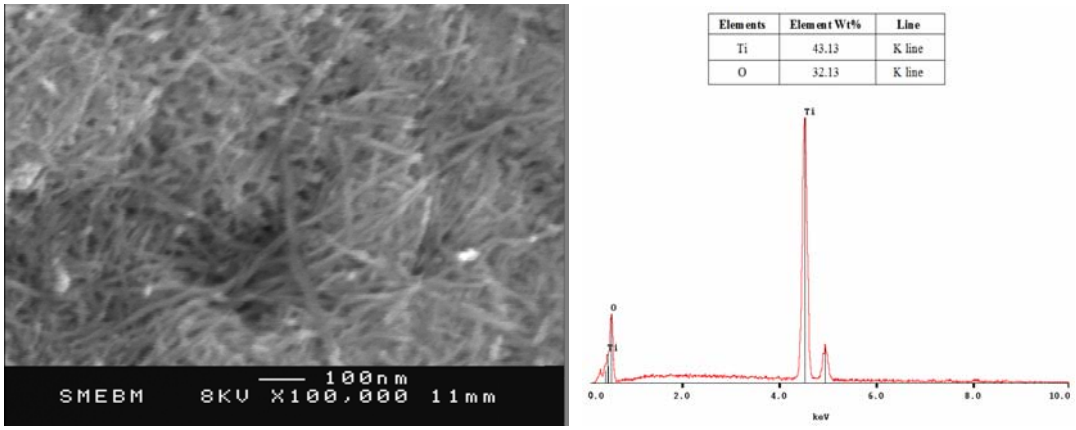


**Fig. 1.** HRSEM image and EDX Spectra of $TiO_2$(B)-nanotubes.

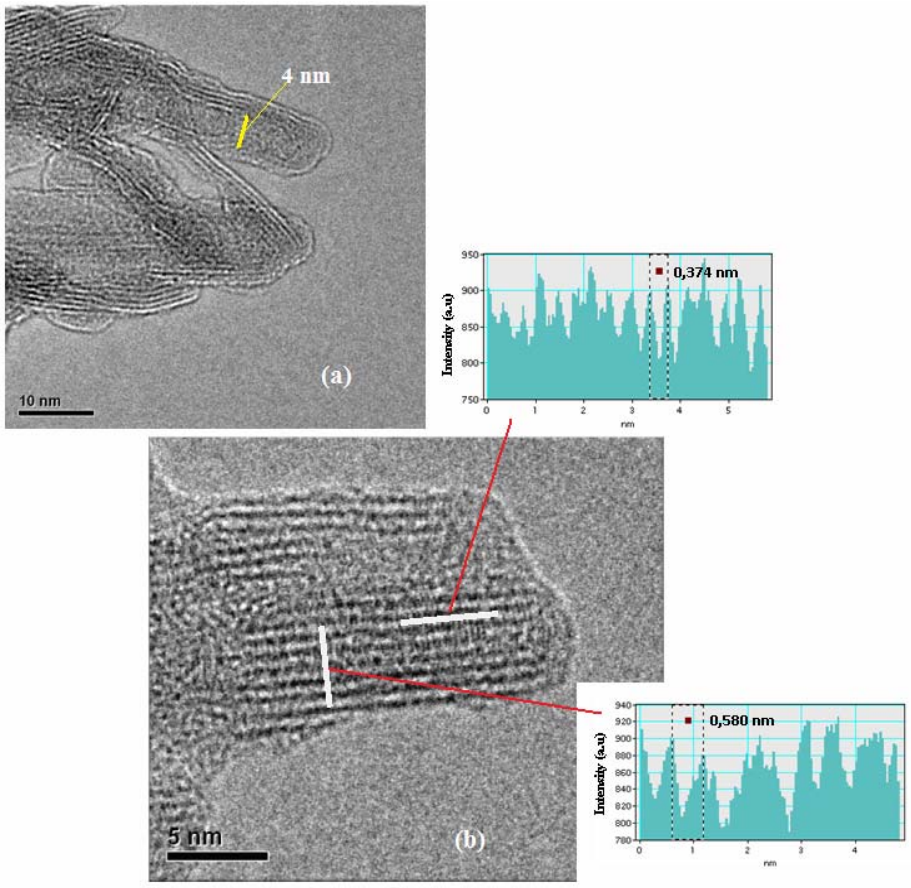


**Fig. 2.** HRTEM Images of $TiO_2$(B)-nanotubes.

The presence and size distribution of tubular materials were shown in the corresponding HRTEM image (Fig. 2a). It clearly shows that the tubular structure are well crystalline tubes, with an inner shell diameter of about 4-5 nm, a shell spacing of about 3-4 nm and an average tube diameter of about 10-12 nm. The structures of different shells are well correlated and the tubes are open ended. Fig. 2b shows the HRTEM image and SAED (selected area electron diffraction) pattern of the obtained products. It is a typical HRTEM image of a nanotube with well-defined structure, growing along the [200] direction. On the SAED patterns in Fig. 2, the nanotube is composed of $TiO_2$(B) structural building units with the phases of (200) and (201) planes from the core of the nanotubes. The fringes which are parallel to the tube axis correspond to an interplannar distance of about 0.580 nm. This set of fringes can correspond to the structural features of cisskewed chains and are characteristic of the $TiO_2$(B) or pseudo-$TiO_2$(B) crystal phase in the [200] direction. This fringe spacing is also comparable to the shell spacing of titania nanotubes reported recently [26-27].

### 3.2. Characterization of $TiO_2$ phases

Fig. 3. depicts the typical XRD pattern collected from the $TiO_2$-nanotubes. The peak at 2θ of 13.12$^o$ corresponding to a d-spacing of 0.89 nm was observed to be the strongest. The broad peaks at 2θ of 13.12, 24.23, 28.40, 31.27 and 48.24$^o$ well correspond to (200), (201), (002), (400), and (402) reflections of the $TiO_2$(B), respectively [27].

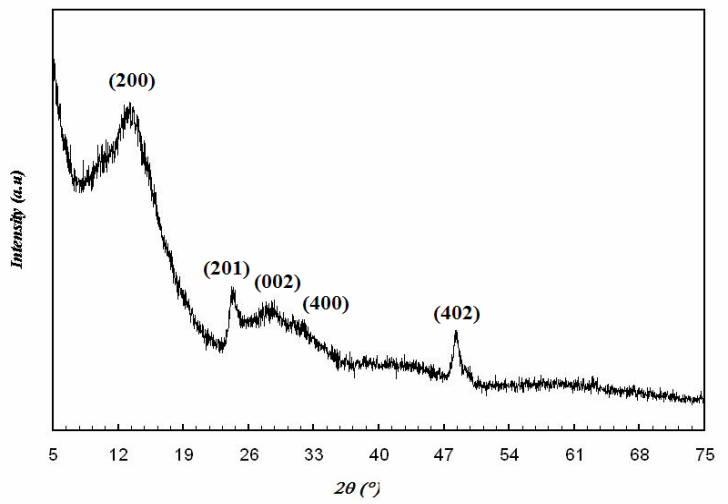


**Fig. 3.** XRD pattern of $TiO_2$(B)-nanotubes.

The XRD patterns of $TiO_2$-nanotubes from various temperatures of sintering are shown in Fig. 4. X-ray diffraction pattern which shows $TiO_2$ nanotubes on the sintering temperatures of 100 to 250 °C is $TiO_2$(B) phase, while those of 300 to 450 °C are indicated two phases: $TiO_2$(B) and anatase, then those of 500 to 650 °C is dominated by anatase phase, and those of 700 to 800 °C are two phases of $TiO_2$: anatase and rutile, then those of 850 to 1000°C is dominated by rutile phase. The main diffraction peaks in Fig. 5a to 5d are as the (200), (201), (002), (400), and (402) reflections of $TiO_2$(B) phase. The main diffraction peaks in Fig. 5i to 5l are indexed as the (101), (103), (200), (105), (211), (213) reflections of crystalline anatase phase, corresponding to those shown in the ICDD card No. 01-075-2550 and the main diffraction peaks (Fig. 4p to 4s) are indexed as the (110), (101), (200), (111), (211) reflections of crystalline rutile phase, corresponding to those shown in the COD card No. 9004141. Formation of rutile phase at high temperatures as this study is in accordance with the results of the work reported by Porozova et al. [28].

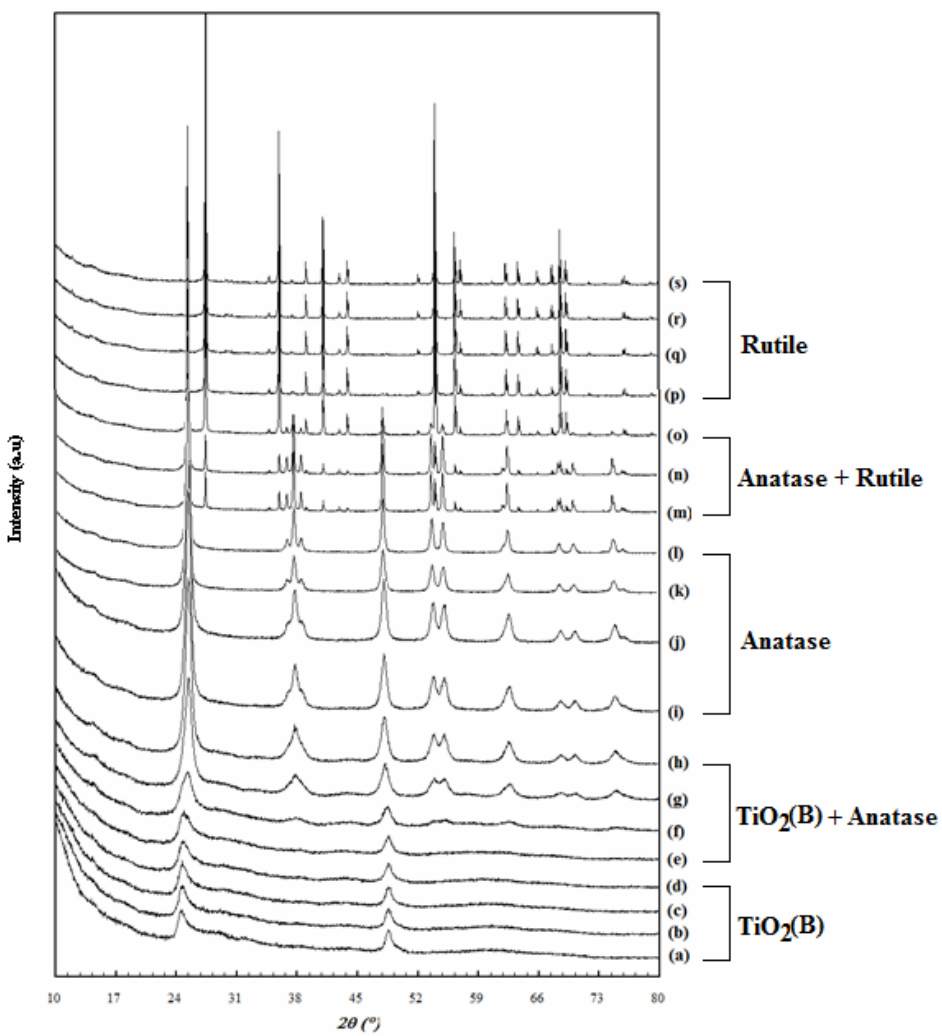


**Fig. 4.** Powder XRD patterns of the $TiO_2$(B)-nanotubes treated under different sintering temperatures: (a). 100 to (s). 1000 °C at interval of 50 °C.

### 3.3 Surface area and pore size distributions of of $TiO_2$-nanotubes

The nitrogen adsorption-desorption isotherm of the obtained product is presented in Fig. 5a. The obtained product shows the type IV isotherm according to the classification developed by deBoer and codified by Brunauer et al. in Condon (2006) [29]. The isotherm type IV represents a capillary condensation phenomenon. The isotherm type is characteristic of a material, which contains mesoporosity and has a high energy of adsorption. These often contain hysteresis attributed to the mesoporosity. The type of hysteresis loop of this material is type H3 according to the classification developed by an IUPAC committee. The hysteresis loop of type H3 is marked by presence the sloping adsorption and desorption branches covering a large range of $P/P_o$ with underlying type II isotherm. Based on type H3, the product has slit-like pores for which adsorbent–adsorbate pair would yield a type II isotherm without pores.

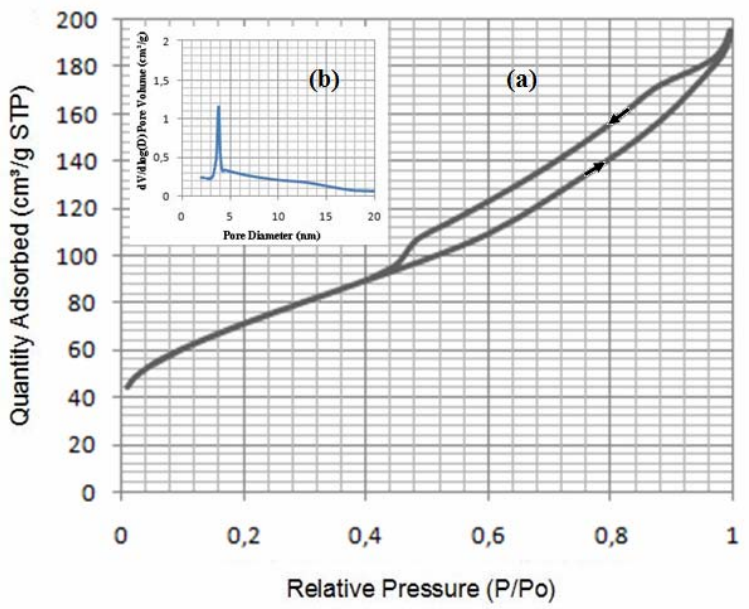


**Fig. 5.** Nitrogen adsorption-desorption isotherms of $TiO_2$(B)-nanotubes.
(*Inset (b): pore size distribution $TiO_2$(B) nanotubes from the adsorption isotherm measurements)*

Fig. 5b shows the corresponding pore size distributions of the $TiO_2$(B) nanotubes. The nanotubes exhibited an average pore diameter of about 4.39 nm. Considering the morphology of the nanotubes observed in Fig. 1 and 2, the smaller pores (< 5 nm) may correspond to the pores inside the nanotubes and the diameters of these pores are equal to the inner diameter of the nanotubes, while the larger pores (10-12 nm) can be attributed to the aggregation of the nanotubes. The pore structures were analyzed further by the BJH method from $N_2$ adsorption–desorption isotherm.

**Tab. I** Surface area, volume and pore size distribution of $TiO_2$(B)-nanotubes from nitrogen adsorption-desorption isotherm measurements.

| Criteria | Value |
|---|---|
| **1. Surface Area ($m^2/g$)** | |
| a. Single point surface area at P/Po ~ 0.300 | 247 |
| b. BET surface area | 253 |
| c. BJH adsorption cumulative surface area of pores (2.00 - 50.00 nm diameter) | 188 |
| d. BJH desorption cumulative surface area of pores (2.00 - 50.00 nm diameter) | 235 |
| **2. Pore Volume ($cm^3/g$)** | |
| a. Single point total pore volume of pores less than ~ 50 nm diameter at P/Po ~ 0.96 | 0,277 |
| b. BJH adsorption cumulative pore volume of pores (2.00 - 50.00 nm diameter) | 0,241 |
| c. BJH desorption cumulative pore volume of pores (2.00 - 50.00 nm diameter) | 0,273 |
| **3. Pore Size (nm)** | |
| a. Average pore diameter (4V/A by BET) | 4,39 |
| b. BJH adsorption average pore diameter (4V/A) | 5,12 |
| c. BJH desorption average pore diameter (4V/A) | 4,64 |

The surface area, pore volume and pore size distribution of the $TiO_2$(B)-nanotubes are summarized in Tab. I. From the Tab., it can be seen that the BET surface area of the $TiO_2$(B)-nanotubes exhibited a maximum surface area of 253 $m^2/g$, corresponding to an average pore diameter of 4.39 nm calculated by the BJH method.

## 4. Conclusion

Based on the obtained results, it can be concluded that the $TiO_2$(B)-nanotubes could be easily synthesized using a simple technique reflux at 150 °C for 24 hours from $Ti(O_2)O.2H_2O$ as a precursor. The $TiO_2$(B) products have nanotubular structures with the diameters of about 10-12 nm in outer and approximately 4-5 nm in inner. The phases of $TiO_2$ obtained from the sintering process of $TiO_2$(B)-nanotubes at 100 to 250°C are indexed as $TiO_2$(B) phase, at 300 to 450 °C are indicated as mixed two phases of $TiO_2$(B) and anatase, at 500 to 650 °C are dominated by anatase phase, and at 700 to 800 °C are indexed two phases of $TiO_2$: anatase and rutile, then at 850 to 1000 °C is dominated by rutile phase.

## Acknowledgements

The authors are pleased to acknowledge the financial supported provided for this research by the Directorate General of Higher Education, Ministry of Education and Culture, Republic of Indonesia based on Hibah Kompetensi No.: 265/SP2H/PP/DP2M/V/2009.

## 5. References

1. A. Loiudice, A. Rizzo, L. De Marco, M. R. Belviso, G. Caputo, P. D. Cozzoli, G. Gigli, Phys. Chem. Chem. Phys., 14 (2012) 3987.
2. P. Yan, X. Wang, X. Zheng, R. Li, J. Han, J. Shi, A. Li, Y. Gan, C. Li, Nano Energy, 15 (2015) 406.
3. Y. Bai, I. Mora-Seró, F. De Angelis, J. Bisquert, P. Wang, *Chem. Rev.,* 114 (2014) 10095.
4. E. Al-Hetlani, M. O. Amin, M. Madkou, Appl. Surf. Sci., 411 (2017) 355.
5. S. Weon, J. Choi, T. Park, W. Choi, Appl. Catal. B: Environ., 205 (2017) 386.
6. U. Joost, K. Juganson, M. Visnapuu, M. Mortimer, A. Kahru, E. Nõmmiste, U. Joost, V. Kisand, A. Ivask, J. Photochem. Photobiol. B: Bio., 12 (2015) 178.
7. Z. Huang, P. C. Maness, D. M. Blake, E. J. Wolfrum, S. Smolinski, W. A., J. Photochem. Photobiol. A: Chem., 130 (2000) 163.
8. S. Hejazi, N. T. Nguyen, A. Mazare, P. Schmuki, Catal. Today, 281(1) (2017) 189.
9. R. Jain, M. Shrivastava, J. Hazard. Mater., 152(1) (2008) 216.
10. N. Miranda-García, S. Suárez, B. Sánchez, J.M. Coronado, S. Malato, M. Ignacio Maldonado, Appl. Catal. B: Environ., 103(3-4) 294.
11. M. Dawson, C. Ribeiro, M. R. Morelli, Ceramics International, 42(1) (2016) 808.
12. S. Banerjee, D. D. Dionysiou, S. C. Pillai, Appl. Catal. B: Environ., 176-177 (2015) 396.
13. X. Ding, S. Zhou, L. Wu, G. Gu, J. Yang, Surf. Coat.Tech., 205(7) (2010) 2554.
14. T. E. Weirich, M. Winterer, S. Seifried, H. Hahn, H. Fuess, Ultramicroscopy, 81(3-4) (2000) 263.
15. R. J. Swope, J. R. Smyth, A. C. Larson, Amer. Mineral., 80 (1995) 448.
16. W. H. Baur, Acta Crystallogr., C14 (1961) 214.
17. T.P. Feist, P. K. Davies, J. Solid State Chem., 101 (1992) 275.

18. J. Yu, H. Yu, B. Cheng, X. Zhao, Q. Zhang, J. Photochem. Photobio. A: Chem., 182(2) (2006) 121.
19. X. Wang, F. Cui, J. Lin, B. Ding, J. Yu, S. S. Al-Deyab, Sens. Actuators B: Chem., 171–172 (2012) 658.
20. E. Comini, V. Galstyan, G. Faglia, E. Bontempi, G. Sberveglieri, Micropor. Mesopor. Mat., 208 (2015) 165.
21. M. A. Hossain, S. Oh, S. Lim, J. Ind. Eng. Chem., 51 (2017) 122.
22. T. Kasuga, M. Hiramatsu, A. Hoson, T. Sekino, K. Niihara, Adv. Mater., 11(15) (1999) 1307.
23. R. L. Rich, Inorganic Reactions in Water, Springer, Heidelberg, 2007.
24. S. Brunauer, P. H. Emmett, E. Teller, *J. Am. Chem. Soc.,* 60(2) (1938) 309.
25. E. P. Barrett, L. G. Joyner, P. P. Halenda, *J. Am. Chem. Soc.,* 3(1) (1951) 373.
26. A. R. Armstrong, G. Amstrong, J. Canales, P. G. Bruce, Angew. Chem. Int. Ed., 43 (2004) 2286.
27. B. D. Yao, Y. F. Chan, X. Y. Zhang, W. F. Zhang, Z. Y. Yang, N. Wang, Applied Physics Letters. 82(2) (2003) 281.
28. S. E. Porozova, A. A. Gurov, M. N. Kachenuk, A. A. Smetkin, O. Yu. Kamenschikov, Science of Sintering, 49 (2017) 99.
29. J. B. Condon, Surface Area and Porosity Determinations by Physisorption: Measurements and Theory, Elsevier, Amsterdam, 2006.

***Садржај:*** *Нанотубе титан-диоксида су припремљене једноставном методом рефлукса. Морфологија и микроструктуре нанотуба карактерисане су различитим методама: високо резолуционом скенирајућом електронском микроскопијом, трансмисионом електронском микроскопијом, рендгенском дифракцијом, спектроскопијом и мерењем специфичне површине. Микроструктуре титан диоксидне фазе добијене синтеровањем нанотуба на различитим температурама од 100 до 1000 $^oC$ 1 сат, испитиване су рендгенском дифракцијом. Анализе добијене HRSEM и HRTEM снимањем, указују да се ради о нанотубама. Нанотубе имају структуру $TiO_2(B)$. Рендгени указују на то да се нанотубе трансормишу из анатаса у рутил услед повећања температуре синтеровања.*
***Кључне речи:*** *титан-диоксид, анатас, рутил, микроструктура, нанотубе.*